Branched glycerol dialkyl glycerol tetraethers and crenarchaeol record post-glacial sea level rise and shifts in sources of terrigenous brGDGTs in the Kara Sea (Arctic Ocean)

Cindy De Jonge[a*], Alina Stadnitskaia[a], GeorgyCherkashov[b], Jaap S. Sinninghe Damsté[a,c]

[a] *Department of Marine Organic Biogeochemistry, NIOZ Royal Netherlands Institute for Sea Research, P.O. Box 59, 1790 AB Den Burg (Texel), The Netherlands*

[b] *All-Russian Research Institute for Geology and Mineral Resources of the World Ocean (VNIIOkeangeologia), Ministry of Natural Resources, Russian Academy of Science, St. Petersburg, Russian Federation*

[c] *Utrecht University, Faculty of Geosciences, P.O. Box 80.021, 3508 TA Utrecht, The Netherlands*

* Corresponding author. *E mail address*: dejonge.cindy@gmail.com (C. De Jonge).

Keywords:Branched GDGT; in-situ production; palaeoclimate reconstruction; Kara Sea

Formatted: Font: (Default) Times New Roman, 11 pt

Formatted: Normal, No bullets or numbering

Formatted: Font: (Default) Times New Roman, 11 pt

ABSTRACT

This study evaluates the GDGT distribution and provenance in sediments(spanning a minimum of 13.3 ka) from~~in~~ the St. Anna Trough (Northern Kara Sea). The site has experienced extensive fluctuation in the delivery of river-derived organic matter (OM), caused by a eustatic change in sea level. This is in line with the record of the concentration of the isoprenoid GDGT, crenarchaeol, produced by marine *Thaumarchaota*, which was~~is~~ low at the bottom of the core, increasing gradually in the most shallow unit. The concentration of branched (br)GDG~~D~~Ts showed~~s~~ an opposite trend and a marked shift in distribution. The deepest sediments (> 10 ka), with a distribution currently encountered in surface sediments in front of the Yenisei River, are characterized by terrigenous~~-derived~~ brGDGTs, whereas the distribution in the shallowest unit (< 10 ka) is strongly influenced by marine, in-situ~~-produced~~ brGDGTs. During the shift from terrigenous to marine-sourced brGDGTs, there was~~is~~ one horizon where a pronounced shift in the brGDGT distribution wa~~i~~s observed and the brGDGT concentration~~s~~ significantly decreased. As the brGDGTs delivered to the current Kara Sea system are derived from several sources, we postulate that a temporary change in the relative importance of the brGDGT sources happened during this interval. Both in-situ production and changing brGDGT provenance have implications for palaeoclimate reconstruction using brGDGTs. In-situ production of marine brGDGTs results in a higher reconstructed pH. However, these in-situ produced brGDGTs di~~d~~e not influence the reconstructed mean annual air temperature (MAT), when the MAT_{mrs} calibration wa~~i~~s used. Changes in the relative contribution of brGDGT sub-pools were shown, however, to influence both soil pH reconstruction and MAT reconstruction.

1. Introduction

Branched glycerol dialkyl glycerol tetraethers (brGDGTs; Fig. 1) are ubiquitous bacterial membrane lipids produced in soils, where their distribution depends on the prevailing mean annual air temperature (MAT) applied on the soils, as well as the soil pH (Weijers et al., 2007). Based on this dependence, brGDGTs have found application as a palaeoclimate proxy for~~in~~ palaeosoils (e.g. Peterse et al., 2011; Zech et al., 2012), lacustrine sediments (e.g. Niemann et al., 2012; Das et al., 2012), but initially for~~in~~ coastal marine sediments that receive a substantial amount of soil-derived matter (Weijers et al., 2007, 2009; Bendle et al., 2010). As brGDGTs are present in high abundance in soils and decrease in concentration in the marine system, their presence in modern and down~~-~~core marine sediments was interpreted to reflect the delivery of soil-derived OM (e.g. Kim et al., 2006; Ménot et al., 2006). For this purpose, the branched and isoprenoid tetraether (BIT) index was developed, where the concentration of terrigenous brGDGTs is calculated relative to the marine thaumarchaeotal lipid crenarchaeol (Hopmans et al., 2004; Fig. 1). Additionally, soil-derived brGDGTs in coastal marine sediments may provide information on past continental climate (Weijers et al., 2007). However, several mechanisms can complicate this. Firstly, brGDGTs have been described to be produced in-situ in marine sediments (e.g. Peterse et al., 2009; Zhu et al., 2011 Zell et al., 2014a,b). These studies generally observed the production of cyclopentane-containing brGDGTs, which was explained by the relatively high pH of the pore~~-~~water~~s~~ of the marine sediments. Secondly, brGDGTs are derived from a variety of watershed soils, where different soil types can carry different distributions, and erosional patterns can change through time. It is thus possible for their soil-derived brGDGT contribution to the river and the marine system to change through time (e.g. Bendle et al., 2010). BrGDGTs are also produced in river water and this has been described to influence or dominate the soil-derived brGDGTs in river systems (e.g. Zell et al., 2013, 2014; Buckles et al., 2014; De Jonge et al., 2014a). This results in a variety of brGDGT sources that can change over time and influence the brGDGT distribution and abundance in marine sediments. In the light of the diversity of the terrigenous sources of brGDGTs, De Jonge et al. (2015a) suggested ~~to~~ interpreting their abundance, and the derived BIT-index values, as indicative of~~for~~ the delivery of terrigenous organic matter (OM), including riverine OM~~organic matter~~, rather than only soil-derived OM~~organic matter~~.

Although the majority of palaeoclimate reconstruction studies has been based on a dataset of 9 brGDGTs, recent analytical developments (De Jonge et al., 2014b) now allow separation of 15 brGDGT compounds (Fig. 1), including six 5-methyl brGDGT ~~compound~~s as described by Sinninghe Damsté at al. (2000) and Weijers et al. (2006), and six recently described 6-methyl compounds (De Jonge et al., 2013; 2014b) that previously co-eluted with the 5-methyl brGDGTs. The 6-methyl compounds were shown to be abundant in the Yenisei River and its outflow into the Kara Sea (De Jonge et al., 2014a, 2015a).

The Kara Sea is a shallow shelf sea connected to the Arctic Ocean. The ~~organic matter (~~OM~~)~~ in its sediments is influenced strongly by river-derived terrigenous material, as indicated by bulk

elemental composition (e.g. Fernandes and Sicre, 2000; Guo et al., 2004; Lein et al., 2012) and by the presence of molecular soil markers in the sediments (e.g. van Dongen et al., 2008; Cooke et al., 2009; Gustaffson et al., 2011; De Jonge et al., 2016). The brGDGT-based BIT index (Sparkes et al., 2015; De Jonge et al., 2015a) revealed the presence of terrigenous bacterial OM in East Siberian Sea and Kara Sea surface sediments, respectively. Based on the distribution of brGDGTs in Kara Sea surface sediments several possible sources were described: i.e. riverine in-situ produced brGDGTs and an unknown contribution of soil-derived and coastal cliff-derived brGDGTs (De Jonge et al., 2015a). In modern Kara Sea sediments, in-situ production of riverine brGDGTs and their preferential degradation was postulated to influence the distributions delivered by the Yenisei River, resulting in large differences in brGDGT-based reconstructed MAT values and soil pH. Whether these mechanisms can have a significant impact on the sedimentary record was not known ~~yet~~.

For this purpose, we have investigated the sedimentary GDGT record of the Kara Sea covering~~for~~ at least the last 13.3kyr. During this period (Late Weichselian and the Holocene) the sea has experienced large shifts in sea level, resultingin a regression in the position of the Yenisei and Ob River mouths. A sediment core was collected from~~in~~ the St. Anna Trough, which~~that~~ was formed by a marine-based glacier during the Last Glacial Maximum (LGM; Polyak et al., 1997). The sedimentological history of the trough has been documented in ~~a number of~~ lithological studies (Polyak et al., 1997; Hald et al., 1999). These studies describe large changes in the sedimentation regime~~s~~ in the trough, shifting from a glacial sedimentation regime dominated by deposition of glacial ice-rafted debris (IRD) and river-derived clastic material, to the modern setting. Here, the GDGT concentration, brGDGT distribution and BIT index are used to track changes in the relative contribution of terrigenous OM and marine OM over time, and to identify th~~eose~~ processes that would~~ill~~ have an impact on the brGDGT distribution in the sedimentary record..

2. Study site

The St. Anna trough is a North to South facing, open ended glacial trough located approximately between 77–82-°N and 65–75-°E at the outer Eurasian continental margin (Fig. 2A, B). It is bounded by the islands of Franz Joseph Land to the west, Novaya Zemlya to the south, the shallow bank area Central Kara Plateau in the east and the Arctic Ocean to the north. It is a major pathway for the export of water, sediment and ice between the Arctic Ocean and the Kara Sea (Stein et al., 2004). The core position is in the southern basin of the trough, 200 km to the northeast of Novaya Zemlya. The polar surface water in the study area (-1.75 to 0 °C, salinity 34-33.2‰; Hald et al., 1999) occupies the upper ca. 100 m of the water column and is formed partly in the Arctic Ocean and partly in the Kara Sea, where fresh-water from the large Siberian rivers (Yenisei, Ob) and from sea ice cover is under the influence of low insolation. During summer, surface salinity is reduced to 32‰ and the temperature may increase by 2–3 °C. Because of its low salinity, the polar surface water forms a lid upon the warmer Atlantic water (Aagaard and Carmack, 1989). This intermediate, Atlantic-derived

water (33‰, 1.5 °C) can move southwards into the trough at a depth from 100 to 400 m (Hanzlick and Aagaard, 1980; Hald et al., 1999). More saline (> 34.60‰; e.g. Hald et al., 1999) polar water is formed below forming sea ice and forms the bottom water in the through (Midttun, 1985). During fall and winter, sea ice forms in the Kara Sea and the eastern and northern part of the Barents Sea (e.g. Aagaard and Carmack, 1989).

During the LGM, the temperature in Siberia was between 7 and 15 °C colder in winter (for both south and north Siberia; Frenzel et al., 1992a; Tarasov et al., 1999), and between 1 to 10 °C colder in summer (for south and north Siberia, respectively; Frenzel et al., 1992b; Tarasov et al., 1999; Osipov et al., 2010), thancompared to modern-day temperatures. In the area of low-elevation Lake Baikal, LGM temperature values were reconstructed to have been 18 °C colder for winter months and 4 °C for summer months (Tarasov et al., 2009). In the period following the LGM, several large changes in the erosion of the Siberian continental soils wearе inferred, caused by the melting of large continental icesheets (i.e. Kleiber and Niessen, 2000).

3. Material and methods

3.1. Sediment collection

The gravity core (3.03m) was collected at 78° 28' 9928 N, 72° 47' 8487 E, at a depth of 473m below sea level, aboard the R/V Akademik Mstislav Keldysh. It was subsampled (n=32) on-board, after a detailed description of the lithology was made. For this purpose, the grain size classification as employed by Shepard et al. (1954) was used. The colour of the sediments was described using a standard Munsell colour chart (Munsell Color ©). Samples were taken from a 1 cm broad slot, where the top of the sediment slot is reported in Table 1 and the Supplementary. Table 1. After subsampling, the sediments were immediately stored at -20 °C.

3.2. Bulk elemental analysis

The homogenized and freeze dried sediments were decalcified in an overnight reaction with 1.5 N HCL solution and rinsed 3x to 5xthree to five times with bidistilled water to aadjust the pH ofto 4-5. After freeze drying and subsampling, the bulk geochemical parameters [total organic carbon (TOC), total nitrogen (TN), stable carbon isotopic composition of organic carbon (δ^{13}Corg), satble nitrogen isotopic composition (δ^{15}N)] were measured usingon a Flash 2000 Organic Elemental Analyzer.

3.3. Lipid extraction and GDGT analysis

Freeze dried, homogenized sediments (2.5 to 3 g) wasere extracted using accelerated solvent extraction (ASE; Dionex), with a 9:1 (v/v) mixture of CH_2Cl_2dichloromethane and MeOHmethanol (100 °C, 3x). The extract was separated according to polarity over activated alumina and the polar fraction analyzed using high performance liquid chromatography-atmospheric pressure chemical ionization-mass spectrometry (HPLC-APCI-MS), as described by De Jonge et al. (2014b). Detection

Formatted: Subscript

Formatted: Subscript

was via selected ion monitoring (SIM; Schouten et al., 2007) using *m/z* 744 for the internal standard, *m/z* 1292 for crenarchaeol and *m/z* 1050, 1048, 1046, 1036, 1034, 1032, 1022, 1020 and 1018 for brGDGTs. Agilent Chemstation software was used to integrate peak areas in the mass chromatograms of the $[M+H]^+$ ions. However, visual inspection revealed that the brGDGT with *m/z* 1020 often co-eluted with an unidentified compound to provide~~present as~~ a broad peak, so its concentration was~~should~~ be interpreted with caution.

3.4. Calculation of GDGT-based proxies

The BIT index was calculated according to Hopmans et al. (2004). The inclusion of 6-methyl brGDGTs (De Jonge et al., 2013) is mentioned explicitly:

BIT index = (Ia+IIa+IIIa+IIa'+IIIa')/(Ia+IIa+IIIa+IIa'+IIIa'+IV). (1)

The roman numerals refer to the fractional abundances of GDGTs in Fig. 1. Here, Ia, IIa and IIIa are 5-Me brGDGTs, IIa' and IIIa' are 6-methyl brGDGTs and IV is the isoprenoid GDGT (iGDGT) crenarchaeol, a GDGT specific for *Thaumarchaeota* (SinninghеDamsté et al., 2002).

The isomer ratio (IR) represents the fractional abundance of the penta- and hexamethylated 6-methyl brGDGTs vs. the total of penta- and hexamethylated brGDGTs (modified after De Jonge et al., 2014a):

IR = (IIabc'+IIIabc')/(IIabc+IIIabc+IIabc'+IIIabc'). (2)

Xabc means that the index includes both the non-cyclopentane containing (Xa) and the cyclopentane containing (Xb,c) components (Fig. 1).

We calculated ~~a~~reconstructed pH using the CBT' index following De Jonge et al. (2014b):

$CBT' = \log_{10}[(Ic+IIa'+IIb'+IIc'+IIIa'+IIIb'+IIIc')/(Ia+IIa+IIIa)]$. (3)

pH = 7.15 + 1.59 x~~*~~ CBT' (4)

The MAT_{mrs} was calculated as a multiple linear regression, based on the abundance of only the major brGDGTs Ia, IIa and IIIa (De Jonge et al., 2014b):

$MAT_{mrs}(°C) = 5.58 + 17.91 \times [Ia] - 18.77 \times [IIa]$ (5)

The square brackets indicate that the fractional abundance of brGDGT Ia and IIa is calculated relative to the sum of the three major brGDGTs (Ia+IIa+IIIa). This calibration was chosen over the MAT_{mr} calibration, which is based on the fractional abundance of the brGDGTs Ia, Ib, Ic and IIa, relative to all 15 brGDGTs, to exclude ~~the~~ brGDGT Ib, which co-eluted with an unknown compound, based on the peak shape.

3.5. Statistical analysis

SThe statistical analysies waseere performed with the software package R (3.2.1.). An unconstrained Q-mode principal component analysies (PCA), based on the correlation matrix, was performed on the standardized fractional abundances of the compounds, using the vegan package (Oksanen et al., 2015). The calculated brGDGT scores calculated are proportional to the eigenvalues, and the site scores were calculated as the sum of the species scores. Squared pearson correlation coefficients (r^2) reported have an associated p -value < 0.05.

4. Results

4.1. Lithology of core

The core (303 cm) consists of a number of clearly defined lithological units (Fig. 3A; Table 1, Supplementary. Table 1), based on a visual description. Underlying a fluffy top layer, a large lithological unit (Unit 1, 0-133 cm below sea floor; bsf) is present, composed of light olive greay (5Y5/2) silty clay; multiple ferrous and shell fragments are present. This unit overlies a second unit (133-210 cm bsf) composed of 4 thin subunits (Unit 2a-d) and a thicker Unit 2e. Unit 2a (133-139 cm bsf) is composed of silty clay laminae. No ferrous iron deposits were encountered in this section.Unit 2b (139-144 cm bsf) is characterized by a slightly different colouration, as it is composed of silty clay sediments with a colour between moderate olive brown (5Y4/4) and light olive brown (5Y5/6). The lower boundary of this section contains an oxidized lens, with an aberrant coloor (OX I). Also, Unit 2c is only a few cm thick (144-148 cm bsf) and is composed of light olive greay (5Y5/2) silty clay. At the bottom of this section a second oxidized lens is present (OX II, ÷ 147.5 – 148 cm bsf), characterized by a moderate yellowish brown (10YR5/4) sandy clay and containing gravel particles and lenses of greyish-black sand. Unit 2d (148 – 155 cm bsf) is a light olive greay (5Y5/2), massive silty clay containing gravel particles. It overlies a much thicker Unit 2e (155-210 cm bsf) composed of a darker, greayish olive (10Y4/2) silty clay, with extensive banded ferrous precipitates. Particularly towards the lower boundary, rock material is present, containing pieces up to 4 cm long. The basal unit of the core, Unit 3 (210 – 303 cm bsf) is described as diamicton and is composed mainly eof sandy clay, with gravel fragments of variable size.

4.2. Downcore variation in bulk OM properties

Total organic carbon (TOC) and total nitrogen (TN) contents, the ratio of TOC/TN (C/N) and the stable OC and N isotopes ($\delta^{13}C_{org}$ and $\delta^{15}N$) were measured to trace potential downcore changes in the delivery of terrigenous and marine OM (Fig. 3B-F, Supplementary. Table 1). The TOC and TN content varied between 0.3 and 1.5% and 0.04 and 0.2 % dry wt, respectively. The highest TOC content was in Unit 2b, the lower part of Unit 2e and the upper part of Unit 3. Furthermore, increased values were encountered in the most recent sediments (Fig. 3B). The TN profile did not mimick the

downcore pattern in TOC completely. Although increased values occurred in recent sediments, the highest TN content was in the upper layers of the diamictic Unit 3. Furthermore, increased values were present in Unit 2a and at the boundary between Unit 2d and 2e (Fig. 3C). Overall, the TOC and TN content down-core did not follow the change in lithology. Values of ~~the~~ C/N ~~ratio~~ (Fig. 3D), commonly used to differentiate between marine and terrigenous OM (e.g. Thornton and McManus, 1994), varied between 7 and 18. The highest values were in Unit 2b and in the deeper part of Unit 2e. They decreased from the bottom to the top of Unit 1, remaining relatively stable in the upper 60 cm bsf. Also, $\delta^{13}C_{org}$ and $\delta^{15}N$ were measured to trace the source of the bulk sedimentary OM (e.g. Krishnamurthy et al., 2001). The $\delta^{13}C_{org}$ had less negative values both in recent sediments and the upper part of diamicticon ~~(~~Unit 3~~)~~. The interval containing the oxidized layers (although the oxidized layers themselves were ~~been~~ sampled) was characterized by more negative $\delta^{13}C_{org}$ values (Fig. 3E). The $\delta^{15}N$ values were lower in horizons with decreased TN content - the lower part of Unit 1, throughout Units 2b, 2c, 2d and in Unit 2e, excluding the boundary between Unit 2d and Unit 2e (Fig. 3F).

4.3. GDGT abundance and distribution

Both brGDGTs and crenarchaeol were present in all the samples (Figs. 3G-H; Table 1). BrGDGTs had TOC-normalized abundance between 7 and 60 µg/gTOC, with the majority of the samples having a concentration < 30µg/g TOC. Crenarchaeol was present in comparable concentration, varying between 3 and 190 µg/g TOC, with substantially higher values in the upper part of the core. Values > 20 µg/g TOC were only encountered in Unit 1 (Fig. 3H). The contrasting down-core behaviour of brGDGTs and crenarachaeol was reflected in a distinct record of the BIT index (Fig. 3I; [Eq. 1]), with values varying between 0.01 and 0.87, with low (< 0.2) onesvalues in Unit 1 and higher ones in all other units. Unit 2d was, however, characterized by lower BITvalues then those of the sandwiching Units 2c and 2e.

To identify the end members of the brGDGT distributions, the variance in brGDGT distribution could be described in a PCA~~principal component analysis~~ (PCA_{SAT}; PCA of St. Anna Trough sediments), based on the standardized abundances of the 15 brGDGTs (Table 1). The first two PCs explained a large part of the variance, explaining 58 and 20% ~~of the variance~~, respectively (Fig. 4A). The first PC ($PC1_{SAT}$) highlighted the good correlation between the fractional abundances of brGDGTs IIIb, IIIc, IIb', IIc', IIIa', IIIb', IIIc' (r^2 varies between 0.57 and 0.95). In general, these fractional abundances possess a negative correlation with that of brGDGT IIa (r^2 varying~~ies~~ between 0.46 and 0.95). The second PC($PC2_{SAT}$) indicated that, for a smaller part of the variance, the fractional abundance of brGDGTs Ia, Ic and IIc followed a different trend, anti-correlating with that of ~~the~~brGDGT IIa' (r^2 between 0.16 and 0.32) and, to a lesser extent, IIIa and IIIa'.

The down-core trends in brGDGTs, as captured by $PC1_{SAT}$ and $PC2_{SAT}$, are shown in Fig. 4B-C. The sediments of Unit 1 all plotted negatively on the first PC, indicating that the brGDGTs with a

negative score on $PC1_{SAT}$ were relatively increased in the shallow sediments.The deeper sediments of Units 2 and 3 all scored positively on $PC1_{SAT}$. In the lower part of Unit 1 the score on PC1 gradually increased towards the values of PC1 in Unit 2 and 3. While the score on $PC2_{SAT}$ was generally constant down-core (Fig. 4C), and close to 0 for the majority of the samples, the distribution at 150 and 153 cmbsf (Unit 2d), had highly negative values on this PC. The contrasting behaviour of the 5- and 6-methyl brGDGTs along PC1 was also reflected in the large variability in IR values (Eq. 2), that generally traced the down-core scores on PC1 (Fig. 4D). This illustrates the necessityof quantifying the 5- and 6-methyl compounds separately when studying down-core brGDGT variation.

Based on the PCA of the brGDGT distributions, we could identify three clear brGDGT end members [Unit 1; Unit 2d (especially 150 and 153 cm bsf) and the remaining sections of Units 2 and 3]. These distributions are exemplified by those at 1, 153 and 200 cm bsf (Figs. 4E-G). The tetramethylated brGDGT Ia was the most abundant at all three depths. The distribution in Unit 1 (Fig. 4E; Table 1) was further characterized by a large fractional abundance of ~~the~~ 6-methyl brGDGTs, with IIb' in larger fractional abundance than IIa', ~~which is~~ an uncommon distribution. The distribution in Unit 2d (Fig. 4F) shows a high fractional abundance of Ia (49-56%), with a low abundance of ~~the~~ 6-methyl brGDGTs. The "deep" distribution (Fig. 4G) was~~showed~~ a contrasting one, dominated by non-cyclopentane containing brGDGTs but with Ia less abundant (< 38%) and with ~~the~~ 5-methyl brGDGTs in higher abundance~~s~~ than the 6-methyl brGDGTs, but not as extreme as in Unit 2d.

To evaluate the distributions down-core with those in suspended particulate matter (SPM) and surface sediments in the Yenisei River and its outflow to the Kara Sea, an extended dataset, composed of the standardized fractional abundances of the 15 brGDGTs in both the modern setting (De Jonge et al., 2015a) and in the down-core trough sediments, was used to calculate PCA_{EXT}. The modern sediments (De Jonge et al., 2015) were collected in the Yenisei Outflow and Kara Sea, between 50 and 600 km form the Yenisei River mouth. The scores on the first two PCs (40 and 23% of the variance, respectively) of both brGDGTs and the various sitesare indicated in Fig. 5. $PC1_{EXT}$ (Fig. 5A) generally captured the same variance as $PC1_{SAT}$ in the PCA of the down-core distributions (Fig. 4A), with cyclopentane-containing Ib, Ic, IIc, IIIb, IIb', IIc', IIIb' and IIIc' having low scores and 5-methyl brGDGTs IIa and IIIa high scores. In particular, the sediments from Unit 1 had a highly negative value on this PC, while the sediments from other units had scores close to 0. $PC2_{EXT}$ captured the different trend in the fractional abundance of brGDGT Ia, and the contrasting behaviour of the 6-methyl brGDGTs IIa' and IIIa'. On this second PC, the scores for the sediments of Units 1 to 2cwere all close to 0, while Units 2e, 3 and 2d had increasingly positive values, reflecting a decrease in the fractional abundance of ~~the~~ IIa' and IIIa', and a corresponding increase in the fractional abundance of Ia. The modern Yenisei River SPM had a highly negative loading on $PC2_{EXT}$, reflecting the high fractional abundance of IIa' and IIIa' (De Jonge et al., 2014a; 2015a).

5. Discussion

5.1. Stratigraphy of core

Although no horizons were dated ~~for the core~~, careful interpolation of the lithological strata with other dated St. Anna Trough cores (Polyak et al., 1997; Hald et al., 1999) allowed~~s~~ deriving an age for a few horizons (Fig. 3A). The deepest facies described by Hald et al. (1999) and Polyak et al. (1997) formed underneath a marine-based glacier, or in association with an ice sheet grounding line, locally disturbed by iceberg tracks. These sediments are present at 140 to > 400 cm bsf in the trough, and at a depth between 150 and >250 cm bsf in cores from the vicinity of our coring site (Hald et al., 1999). The lithology of these sediments was described to be a massive diamicton with a high sand content (Polyak et al., 1997). The similar lithology and depth at the deepest unit in our core (Unit 3; 210 cm bsf) indicate that this unit probably corresponds with the deepest horizons encountered in Polyak et al. (1997) and Hald et al. (1999).

These authors further postulated that the top of this unit was formed during the onset of the ice retreat, that had a minimum age of 13.3 ka in the trough. In the core here, this transition is probably the boundary between Unit 3 and Unit 2e. Overlying this basal unit, an intermediate section was described by Polyak et al. (1997) of < 1 m in thickness, ~~that is~~ comprisinged ~~of~~ several lithological units, wherein alternating glacial deposits were described, whose characteristics indicated forwards and backwards shifts in the proximity of the trough and Novaya Zemlya glaciers (Hald et al., 1999). The heterogeneity within the intermediate unit in our core (Unit 2), thus probably reflects the complex deglaciation sequence on Novaya Zemlya and in the trough. In these transitional horizons, Hald et al. (1999) reported the presence of laminations, indicating the periodic input of sediments, with little bioturbation. Similar laminations occur in Unit 2a. Another feature ~~found~~ throughout the trough (Polyak et al., 1997) is the presence of clear oxidized lenses within this section. Their formation suggests a relatively low deposition rate and oxic bottom waters, perhaps associated with a reduction in calving/melting of the glacier front, or with a permanent sea-ice cover (Hebbeln and Wefer, 1991; Polyak et al., 1997). In the Bering Strait, the presence of oxidized layers in the sediments was related to the presence of substantial amounts of seasonal sea ice, associated with ~~a~~ decreased organic productivity during summer and intensive downwelling of O_2-rich brine during the winter months (Gardner et al., 1982). Two oxidized lenses are described in this core (OX I and OXII), based on the characteristic brown colour of the oxidized sediments. The colour shift can be attributed to the formation of Mn and Fe oxides, and the dissolution of biogenic carbonate~~s~~ in the subsurface sediment (e.g. Wilson et al., 1986), although downcore oxidized layers (6 ka) from the Bering Strait were described only as being enriched in Mn (Gardner et al., 1982). The widespread presence of two oxidized beds and two sandy beds~~,~~ resulted in their use as lithostratigraphic markers (Polyak et al., 1999). One oxidised layer was especially easily recognized, as it was described to directly overlie a dark gre~~a~~y sandy bed. It was dated as being deposited between 10 and 11 ka, by extrapolation of available radiocarbon ages in Polyak et al. (1997). Based on the similar lithology, we propose that the

layer OXII, overlying a distinct sandy bed (147.5-148 cm bsf; Unit 2c), was deposited at an estimated age of 10.5 ka in this core.

The upper unit in the trough has been described by both Polyak et al. (1997) and Hald et al. (1999) to be a homogenous, soft clayey mud, lacking glacial deposits and deposited under similar oceanic conditions as observed today. Overlying an initial phase with increased sedimentation speed related to a lower sea level, increased coastal erosion, and increased river discharge, an oxidized layer was described within the upper unit (Polyak et al., 1997) inferred to have an age of 8 ka. However, if this age is interpolated for the OXI layer in our core, Late Holocene sediments would have a linear sedimentation rate of 18 cm/kyr, while the Early Holocene sediments would have a linear sedimentation rate of only 1.6 cm/kyr. We thus postulate that the oxidized front in cores collected deeper in the trough (> 600 m) is not observed here. Based on the homogenous nature of Unit 1, we postulate that the onset of the marine sedimentation regime, dated around 10 ka (e.g. Polyak et al., 1997), is coeval with the formation of the lower boundary of Unit 1. As the fluffy nature of the surface sediments indicates that the gravity core was successful in collecting the most recent sediment, the top of the core is assumed to be of a recent age (0 ka).

Based on the four dating points (Fig. 3A), the linear sedimentation rate is estimated to be 14 cm/kyr for the modern sedimentation regime (average for Unit 1), amounting up to 23 (average for Unit 2a, b, c) and 24 cm/kyr (average for Unit 2d, e) for deeper sediments. This agrees with the average Holocene sedimentation rate estimated to approach 12 cm/kyr for a core sampled close to the study site (0-11 ka; Stein et al., 2004). These authors further stated that the sedimentation rate during the Early Holocene (roughly corresponding with Unit 2), exceeded the sedimentation rate in the Late Holocene, corresponding roughly with Unit 1). Thus, although our dated horizons are based only on interpolated radiocarbon ages, the resulting linear sedimentation rates agree well with published values, and we are therefore confident that we are evaluating a minimum of 13.3 ka of sedimentation in the trough.

5.2. Terrigenous and marine sources of brGDGTs

Based on GDGT concentrations and ~~the~~ BIT index values (Hopmans et al., 2004: Table 1), three main phases could be identified in the trough sediments (Fig. 3G, H, I):(i) high brGDGT and low crenarchaeol concentrations and high (> 0.7)BIT values throughout Unit 2e and Unit 3, (ii) low brGDGTconcentration and increasing crenarchaeol concentration resulting in decreasing, generally low (< 0.2) BIT values in Unit 1 and (iii) low crenarchaeol concentration and variable brGDGT concentration and BIT values in Units 2a-2d. The latter section reflects a transitional zone between Unit 3 and 2e and Unit 1.

The highest brGDGT concentration in Unit 2e (up to 50 µg/g TOC)~~,~~ approaches the concentration in front of the Yenisei River Mouth in surface sediments (i.e. between 12and 87µg/g TOC; De Jonge et al., 2015a). The concentration of the marine end member, crenarchaeol, is low

throughout Units 2e to 3 (< 5 µg/g TOC), comparable with the concentration in surface sediments in front of the Yenisei RiverMouth (between 0.2 and 20µg/g TOC; De Jonge et al., 2015a). Although the brGDGT concentration in the basal sediments (Unit 3) is lower than in Unit 2e, the resulting BIT values in both units vary between 0.7 and 0.85. These values are comparable with BIT values for modern Yenisei Gulf surface sediments, between 200 and 300 km from the river mouth (De Jonge et al., 2015a). Assuming a sea level drop of 50 m at 11 ka (Fairbanks et al., 1989; Bauch et al., 2001), the distance between the core location and the presumed mouth of the paleo Yenisei and Ob Rivers (Stein et al., 2004; Dittmers et al., 2008) was ca. 350 km. The brGDGT concentration and crenarchaeol concentration in Units 2e and 3 thus reflect a setting where the core site was much closer to the Yenisei River mMouth. We couldan further constrain the source of the brGDGTs in Unit 2e and Unit 3 by studying their distribution (Fig. 4). The sediments in Unit 2e and 3 have a similar brGDGT fingerprint, as reflected in their similar scores on both $PC1_{SAT}$ and $PC2_{SAT}$. Compared with the brGDGT distribution in modern Yenisei and Kara Sea sediments and SPM, Units 2e and 3 have similar scores on $PC1_{EXT}$ and $PC2_{EXT}$ (and thus similar brGDGT distributions; Fig. 5B) as the Yenisei Gulf samples, although the distribution encountered in Unit 3 in particular shows an enrichment in the brGDGTs, with a high score on $PC2_{EXT}$ (increase in brGDGT Ia). Thus, the brGDGT concentration, as well as the high BIT index values and the comparable brGDGT distributions reflect the deposition of brGDGTs in a setting where the core site was significantly closer to the mouth of the paleo-rivers Yenisei and Ob, comparable with the current situation in the Yenisei Gulf (ca. 250 km from the river mouth), where riverine transport delivered brGDGTs with a comparable distribution as in the modern Yenisei River Gulf sediments.

A contrasting GDGT content is present in the most recent sedimentary horizon, Unit 1. It contrasts with Units 2d and 3, as it is characterized by low (< 0.2) BIT values that are caused by a strongly decreased amount of brGDGTs and a crenarchaeol concentration that increases from the bottom to the top of this unit, reaching maximum levels at 100 cm bsf (Fig. 3H). The brGDGT concentrations (5-20 µg/g TOC) and BIT values (between 0.05 and 0.1) in this unit are similar to the modern values encountered in offshore sediments in the Kara Sea (i.e. 4 - 20 µg/g TOC and BIT values down to 0.09; De Jonge et al., 2015a), suggesting that conditions during this period resemble those of the current marine system throughout most of Unit 1. However, the crenarchaeol concentration (30-180 µg/g TOC) is significantly higher than in modern Kara Sea sediments, which are 30 µg/g TOC at the maximum (De Jonge et al., 2015a). They are more comparable with the crenarchaeol concentrations in the East Siberian Sea (varying between 38 ± 8 µg/g TOC in the river outflow to 358 ± 65 µg/g TOC at 300-400 km from the river mouths; Sparkes et al., 2015).

Regarding distributions, Unit 1 has highly negative values ofn $PC1_{SAT}$ (Fig. 4B), with increased amounts of the cyclopentane-containing Ib, IIb, IIc, IIIb, IIIc, IIb', IIc', IIIa', IIIb' and IIIc' (Fig. 4A). The downcore decrease in the scores on $PC1_{SAT}$ reflects the increase in concentration of the marine iGDGT crenarchaeol (r^2= 0.85), a specific biomarker for marine *Thaumarchaeota*, reflecting the

increased production of these cyclopentane-containing brGDGTs in a system with increasing marine in situ production. SPrevious studies have used in situ production of brGDGTs in the marine coastal and distal sediments to invoke changing brGDGT distributions compared with the brGDGTs delivered from the continent (Svalbard Fjord, Peterse et al., 2009; Yangtze River, Zhu et al., 2011; Pearl River, Zhang et al., 2012; Tagus River and Amazon River; Zell et al., 2014a,b) and in off-shore marine sediments (Weijers et al., 2014). Overall, these authors describe an increase in the fractional abundance of one or more cyclopentane-containing brGDGTs. As such, in situ production of marine brGDGTs is in line with the observed increase of the cyclopentane-containing brGDGTs along $PC1_{SAT}$ (Fig. 4A).Although minor cyclopentane containing brGDGTs were often below detection limit in the modern Kara Sea sediments, in situ production was shown to increase the cyclopentane-containing Ib, Ic, IIb, IIc, IIIb, IIIc and IIc', which generally agrees with the increase in these brGDGTs in Unit 1. The gradually increasing marine signature of brGDGTs, as observed in the decreasing values ofn $PC1_{SAT}$, the increasing crenarchaeol concentration and the decreasing BIT values indicate an increasingly marine influence on the southern trough during deposition of Unit 1. Indeed, the rise in sea level has been documented to continue until between 5 and 8 ka (Bauch et al., 2001 and Stein et al., 2004, respectively) and can thus be traced in the lower part of the sediments in Unit 1.

The palaeoenvironmental changes from the Units 2e and 3, with a strong river-derived terrigenous sedimentary signal to Unit 1, with a stronger marine signal, can clearly be recognized from the GDGT concentration and distributions andis consistent with evidence based on sediment core and seismic reflection data (e.g. Polyak et al., 2000; Stein et al., 2004). Units 2a-2d reflect the main phase of transition from one phase to the other, although some changes are evident in the upper part of Unit 2e (i.e. start of the decrease in BIT index values; Fig. 3I) and the lowermost part of Unit 1 (i.e. increase in crenarchaeol concentration; Fig. 3H). In Units 2a-2d, the crenarchaeol concentration is still low, but the brGDGT concentration and resulting BIT index values show distinct trends. The relatively high brGDGT concentration in Unit 2e decreases strongly in Unit 2d, but increases in Unit 2c again, before the onset of the gradual decrease in Unit 2b and 2a, that continues into the lowest part of Unit 1. Since the concentration of the marine iGDGT, crenarchaeol, is low throughout these units, and the scores on the $PC1_{SAT}$ remain high, there is no indication for a contribution of marine in-situ produced brGDGTs in the sediments of Unit 2. In Units 2a-c the brGDGT distributions are similar to the terrigenous, river-derived brGDGTs in Units 2e and 3, as they have similar scores on $PC1_{SAT}$ and $PC2_{SAT}$. This indicates that the contribution of river-derived terrigenous brGDGTs remains strong in these sediments. However, the strong decrease in brGDGT concentration in Unit 2d corresponds with a remarkable shift in the distribution, that is characterized by a shift along the $PC2_{SAT}$ (Fig. 4C), most apparent from the substantial increase in the fractional abundance of brGDGT Ia. We postulate that the strong shift in the brGDGT distribution in Unit 2d is related to a shift in the provenance of terrigenous brGDGTs. The brGDGT signature in the modern Kara Sea sediments iwas described to be a mixture of riverine in-situ produced, soil-derived and coastalcliff derived brGDGTs (De Jonge et al.,

2015a). These different sources, but also different sub-pools of brGDGTs within the Yenisei River watershed, are characterized by different distributions and BITvalues (De Jonge et al., 2015a). Enrichment of a brGDGT sub-pool can happen before or after deposition in the sediments. First, a change in the relative contribution of the sub-pools can happen during soil and coastal clifferosion and riverine transport, prior to their delivery to the marine system. Second, the brGDGT distribution of terrigenous OM can be modified after its delivery to the marine system, if the various brGDGT sub-pools differ in degradability. The in-situ production of brGDGT Ia in marine sediments is unlikely, as it (i) does not follow the proposed trend of~~in~~ increasing marine conditions in this core and (ii) disagrees with the global pattern where cold and high pH environments favour the production of highly branched and cyclopentane containing brGDGTs compounds (De Jonge et al., 2014b).

Whether the changing brGDGT distribution in Unit 2dcan be explained by a shift in brGDGT source~~s~~ before burial in the sediments, may be constrained by comparing this distribution with the modern brGDGT signatures of~~in~~ the Kara Sea (Fig. 5B). However, the high score of Unit 2d on $PC2_{EXT}$, driven by the large fractional abundance of Ia, sets it apart from all the modern distributions. They contrast especially with the distribution produced in situ in the Yenisei River SPM, where the fractional abundance of the 6-methyl brGDGTs IIa' and IIIa' is strongly increased, and the fractional abundance of Ia is decreased. Based on PCA_{SAT} and PCA_{EXT}, the shift in brGDGT distribution can thus possibly be caused by an increased contribution of a brGDGT sub-pool predominantly enriched in Ia, or asubstantial decrease in the contribution of riverine in-situ produced brGDGTs, characterized by a relatively high abundance of 6-methyl brGDGTs. A temporary increase in the erosion of continental brGDGTs during the Early Holocene, possibly limited to only part of the Yenisei watershed, or a decrease in the production of in-situ produced brGDGTs may be related to the increased soil erosion during the deglaciation. Indeed, a 'peak' in meltwater runoff, dated between 10 and 13ka, was recognized in the Laptev Sea sedimentary record (Kleiber and Niessen, 2000). This observation was based on an increase in magnetic minerals sourced by the basaltic Putoran Massif, a plateau in the northern reaches of the Yenisei River watershed that was glaciated during the LGM.The brGDGT distribution in a peat overlying a buried glacier at a similar latitude as the Putoran Massif~~,~~ is similar to the distribution in Unit 2d (Fig. 4F), as it is also characterized by a high fractional abundance of Ia (63%; De Jonge et al., 2015a). However, as the geographical extent of brGDGT sub-pools enriched in Ia is unknown, we can~~-~~not constrain whether or not this meltwater pulse may have influenced the brGDGTs delivered to the Kara Sea during the formation of Unit 2d.

Post-depositional modification of brGDGTs is a second mechanism that can enrich a brGDGT subpool. The presence of oxidized lenses in Unit 2 of the Kara Sea sediments (Fig. 3A) reflects a marine system wherein post-depositional oxic degradation may have modified to a variable extent the OM delivered to the site ~~to a variable extent~~. Unit 2d directly underlies OXII (which was not analysed, preventing direct analysis of the impact of the oxidation on brGDGT distribution), an oxidized lens present throughout the Kara Sea. The bulk OM parameters for~~in~~ the sediments underlying this

oxidized lens~~,~~ indicate that O_2 possibly penetrated the surface sediments during the formation of the oxidized front, and possibly oxidized the brGDGT distribution in the subsurface. This is reflected in a slight decrease in~~of~~ TOC and TN, from 1 to 0.6% and from 0.08 to 0.06% respectively (Fig. 3B, C). A shift in the $\delta^{13}C_{org}$ and $\delta^{15}N$ values at the depths of the oxidized lenses, from -24.5 to -26.0 ‰ and from 5.0 to 3.5 ‰ respectively (Fig. 3E, F), can also be attributed to degradation of the OM present in the sediments (e.g. Lehmann et al., 2002; Prahl et al., 2003; Robinson et al., 2012). The effect of degradation is also reflected in the C/N ratio (Fig. 3D), where increased values may reflect degradation of OM (e.g. Mariotti et al., 1984; Thornton and McManus, 1994). However, the extent of degradation, based on the bulk OM proxies, does not completely agree with the interval in the core where a different brGDGT provenance is apparent~~observed~~. Furthermore, ~~previous~~ studies on the effect of oxic degradation on GDGTs, indicated a strong increase in the BIT_index in oxidized sediments, following the preferential degradation of marine in-situ produced crenarchaeol (Huguet et al., 2008; Lengger et al., 2013). The decreasing BIT_values in Unit 2d can only be caused by oxic degradation if crenarchaeol is dominantly derived from terrigenous sources, and differs between brGDGT sub-pools. Nonetheless, preferential degradation was inferred to explain the increase in brGDGT Ia in offshore Kara Sea sediments, and was thus already inferred to act on the brGDGT distribution during transport and incorporation into the sediments (De Jonge et al., 2015a). The increase in the fractional abundance of Ia, Ic and IIcin Unit 2d indicates that a similar mechanism may further influence the distribution delivered to a marine sediment. Furthermore, if degradation acts on the distribution, it would beexpected to act specifically on the brGDGTs produced in-situ in the Yenisei River, as this modern brGDGT pool would~~ill~~ be degraded preferentially, as modern OM has less physical protection against degradation (Blair and Aller, 2012; Arndt et al., 2013). The contrasting score on $PC2_{EXT}$ of the Yenisei River SPM and Unit 2d distributions, respectively, indicates that brGDGTs IIa' and IIIa', ~~that are~~ strongly enriched in the Yenisei River SPM, have a decreased fractional abundance in Unit 2d. This observation_can be explained by invoking~~the mechanism of~~ preferential degradation. Although we do not know the mechanism causing the ~~observed~~ shift in the provenance of terrigenous brGDGTs, the score on $PC2_{EXT}$_may reflect this shift. Thus, the brGDGT distribution fro~~of~~ Unit 2d represents the most intensely enriched/degraded distribution encountered in the modern and down core Kara Sea distributions.

5.3. Implications for brGDGT-based palaeoclimate reconstruction

In the modern Kara Sea SPM and sediments, the brGDGT distribution was shown to be influenced by in-situ production and by a contribution from~~of~~ several terrestrial sub-pools of brGDGTs (De Jonge et al., 2015a). In recent sediments, preferential degradation of a labile brGDGT pool, e.g. the in-situ produced riverine brGDGTs, and possibly also less refractory sub-pools of soil-derived brGDGTs was inferred to explain the changing provenance of brGDGTs in offshore sediments. This study indicates that these processes can also act on longer timescales. The in-situ production of

marine brGDGTs was shown to happen at the same depth as the increase in the marine iGDGT crenarchaeol, and both parameters trace the production of marine OM and the increasingly marine nature of the St. Anna Trough. Although in-situ production in sediments apparently did not influence the brGDGT distributions in Unit 2 and 3, these were in ~~their~~ turn influenced by changes in the provenance of the terrigenous brGDGTs.

To evaluate the influence these various processes may have on the brGDGT-based palaeoclimate distributions, we can evaluate the reconstructed pH and MAT (Fig. 6). For pH reconstruction, we employed the CBT' calibration, a calibration based on a log ratio (Eqs. 3 and 4) of the 6-methyl brGDGTs IIa', IIb', IIc', IIIa', IIIb' and IIIc' and brGDGT Ic, relative to Ia, IIa and IIIa. The MAT temperature was reconstructed using MAT_{mrs} (Eq. 5), that is based only on the abundance of the three major non-cyclopentane containing brGDGTs Ia, IIa and IIIa, as brGDGT Ib was found to co-elute with an unknown compound in some samples (n=15). Both ~~these~~ calibrations are based on a dataset of globally distributed soils (De Jonge et al., 2014b). Overall, the reconstructed pH is relatively stable throughout Units 3 and 2e (between 5.9 and 6.3), decreases sharply in Unit 2d to a pH of 5.8 and subsequently increases in the transitional Units 2c-a towards constant values of ca. 7.1 in Unit 1.Both in-situ production of marine brGDGTs and changes in the provenance of terrigenous brGDGTs would~~ill~~ have an effect on the reconstructed pH. BrGDGTs produced predominantly ~~produced~~ in situ in the marine sediments (i.e. Unit 1) reflect the increased pH of the marine production site, although the reconstructed pH still underestimates the marine (pore)water pH, that is typically between7.8 and~~to~~ 8.4 (e.g. Polukhin and Makkaveev, 2014). An extended dataset of brGDGTs in marine sediments, that were inferred to be in-situ produced in the sediments (Weijers et al., 2014), reported reconstructed pH values between 6.1 and 9.9. These authors postulated that the brGDGT distribution possibly reflected the more variable sedimentary porewater pH values, rather than the more stable pH of the water column. Furthermore, this apparent offset may be due to the fact that the soil pH calibration may not be applicable to marine in-situ produced brGDGTs. Alternatively, it may also indicate that the brGDGTs in Unit 1 represent a mixture of in-situ produced and terrestrial brGDGTs. The sediments in Unit 2d and 3 resemble the current brGDGT distribution in the Yenisei Gulf, and thus reflect a mixture of riverine in-situ produced and coastal-cliff derived brGDGTs. The brGDGT distribution in Unit 2d probably represents a strongly enriched brGDGT sub-pool. The reconstructed pH in this unit approaches the average pH encountered in the watershed soils (5; De Jonge et al., 2014a).

Based on a soil calibration, the reconstructed temperatures in the deepest part of the core (Units 2d and 3; between 6 and 9 °C) are slightly below those calculated for Unit 1 (between 8 and 11 °C). The distinct brGDGT distribution in Unit 2d results in a strongly increased reconstructed MAT at these depths (13-16 °C). As the increase in cyclopentane-containing and 6-methyl brGDGTs, typical for marine in situ production, does not influence the MAT_{mrs}-based temperatures, it may possibly be an appropriate palaeothermometer for the reconstruction of temperature~~s~~ in marine sediments where in situ production is probable.The muted change in temperature since the LGM (± 2 °C) when compared

with~~to~~ previous reconstructions (6-12 °C; e.g. Frenzel et al., 1992a, 1992b) is possibly due to the problematic reconstruction of the MAT from~~in~~ frozen soils (De Jonge et al., 2015a). However, the effect of a changing provenance of terrigenous brGDGTs, as exemplified in Unit 2d, has a large effect (> 4 °C) on the reconstructed temperature in the Kara Sea system. As in-situ production of riverine brGDGTs has been documented in rivers globally (e.g. Kim et al., 2012; Zell et al., 2014a, 2014b) and the watershed of large rivers drains several different soil types, the brGDGT distribution delivered to the marine system globally can be assumed to consist of several sub-pools with different brGDGT distribution. In the case these sub-pools are exported to a different extent on a geological timescale, or if they differ in degradability, this mechanism has to be taken into account when reconstructing palaeotemperature values in shelf seas around the globe.

6. Conclusions

The brGDGT distribution in the St. Anna Trough reveals large changes in terrigenous material delivered since the last regression of marine glaciers from the trough (minimum age 13.3 ka). The brGDGT and crenarchaeol concentration and the BIT index reflect the transition from a sedimentation regime during a sealevel lowstand, where the proximity of the palaeo Yenisei River mouth and Ob River mouth to the core site results in a strong signal from terrigenous river-derived brGDGTs. The rising sea level caused the increase in~~of~~ the fractional abundance of marine in-situ produced brGDGTs (Ib, IIb, IIc, IIIb, IIIc, IIb', IIc', IIIa', IIIb' and IIIc') and absolute concentration of crenarchaeol. This increase in marine production is reflected in an increase in the marine in-situ produced brGDGTs. A clear shift in the provenance of terrigenous brGDGTs can be observed at a depth of 150-153 cm bsf, characterized by an increase in the fractional abundance of predominantly brGDGT Ia. The mechanism causing this shift is unknown as both increased continental erosion and increased degradation in the marine sediments can result in this enrichment.

Both in-situ production of brGDGTs and shifts in the provenance of terrigenous brGDGTs have to be taken into account when reconstructing continental palaeoenvironments. Separating these processes from palaeoclimate-induced changes is a challenge for palaeoclimate reconstruction that can only be solved using a multi-proxy approach involving several (lipid-based) biomarkers and sedimentary characteristics.

Acknowledgments

We thank ~~Dr.B. van Dongen and~~ two anonymous reviewers for comments on an earlier version of the~~is~~ manuscript. We acknowledge the work of A. Mets and J.Ossebaar in ~~the~~ processing ~~of~~ the samples and E.C. Hopmans for helpful discussions. The work was performed in the framework of the memorandum NIOZ-VNIIO keangeologia for Arctic research. The research was funded by research project 819.01.013, financed by the Netherlands Organization for Scientific Research (NWO) and the

European Research Council under the EU Seventh Framework Programme (FP7/2007-2013)/ERC grant agreement No. 226600.

Associate Editor – **B.E. van Dongen**

Formatted: Font: Italic

Formatted: Font: Bold

References

Aagaard, K., Carmack, E.C., 1989. The role of sea ice and other fresh water in the Arctic circulation. Journal of Geophysical Research-Oceans 94, 14485–14498.

Arndt, S., Jørgensen, B.B., LaRowe, D.E., Middelburg, J.J., Pancost, R.D., Regnier, P., 2013. Quantifying the degradation of organic matter in marine sediments: A review and synthesis. Earth and Science Reviews 123, 53–86.

Bauch, H., Mueller-Lupp, T., Taldenkova, E., Spielhagen, R., Kassens, H., Grootes, P., Thiede, J., Heinemeier, J., Petryashov, V., 2001. Chronology of the Holocene transgression at the North Siberian margin. Global and Planetary Change 31, 125–139.

Bendle, J.A., Weijers, J.W.H., Maslin, M.A., Sinninghe Damsté, J.S., Schouten, S., Hopmans, E.C., Boot, C.S., Pancost, R.D., 2010. Major changes in glacial and Holocene terrestrial temperatures and sources of organic carbon recorded in the Amazon fan by tetraether lipids. Geochemistry Geophysics Geosystems 11, Q12007.

Blair, N.E., Aller, R.C., 2012. The fate of terrestrial organic carbon in the marine environment. Annual Review of Marine Science 4, 401–423.

Boucsein, B., Knies, J., Stein, R., 2002. Organic matter deposition along the Kara and Laptev Seas continental margin (eastern Arctic Ocean) during last deglaciation and Holocene: evidence from organic–geochemical and petrographical data. Marine Geology 183, 67–87.

Buckles, L.K., Weijers, J.W.H., Tran, X.-M., Waldron, S., Sinninghe Damsté, J.S., 2014. Provenance of tetraether membrane lipids in a large temperate lake (Loch Lomond, UK): implications for glycerol dialkyl glycerol tetraether (GDGT)-based palaeothermometry. Biogeosciences 11, 5539–5563.

Cooke, M. P., van Dongen, B. E., Talbot, H. M., Semiletov, I., Shakhova, N., Guo, L., Gustafsson, Ö., 2009.Bacteriohopanepolyol biomarker composition of organic matter exported to the Arctic Ocean by seven of the major Arctic rivers. Organic Geochemistry 40, 1151–1159.

Das, S.K., Bendle, J., Routh, J., 2012. Evaluating branched tetraether lipid-based palaeotemperature proxies in an urban, hyper-eutrophic polluted lake in South Africa. OrganicGeochemistry 53, 45–51.

De Jonge, C., Hopmans, E.C., Stadnitskaia, A., Rijpstra, W.I.C., Hofland, R., Tegelaar, E., Sinninghe Damsté, J.S., 2013. Identification of novel penta- and hexamethylated branched glycerol dialkyl glycerol tetraethers in peat using HPLC–MS^2, GC–MS and GC–SMB-MS. Organic Geochemistry 54, 78–82.

De Jonge, C., Hopmans, E.C., Zell, C.I., Kim, J.-H., Schouten, S., Sinninghe Damsté, J.S., 2014a. Occurrence and abundance of 6-methyl branched glycerol dialkyl glycerol tetraethers in soils: Implications for palaeoclimate reconstruction. Geochimica et CosmochimicaActa 141, 97–112.

De Jonge, C., Stadnitskaia, A., Hopmans, E.C., Cherkashov, G., Fedotov, A., Sinninghe Damsté, J.S., 2014b. In situ produced branched glycerol dialkyl glycerol tetraethers in suspended particulate matter from the Yenisei River, Eastern Siberia. Geochimica et CosmochimicaActa 125, 476–491.

De Jonge, C., Stadnitskaia, A., Hopmans, E.C., Cherkashov, G., Fedotov, A., Streletskaya, I.D., Vasiliev, A.A., Sinninghe Damsté, J. S., 2015a. Drastic changes in the distribution of branched tetraether lipids in suspended matter and sediments from the Yenisei River and Kara Sea

(Siberia): Implications for the use of brGDGT-based proxies in coastal marine sediments. Geochimica et CosmochimicaActa165, 200-225.

De Jonge, C., Talbot, H.M., Bischoff, J., Stadnitskaia, A., Cherkashov, G., Sinninghe Damsté, J.S., 2016. Bacteriohopanepolyol distribution in Yenisei River and Kara Sea suspended particulate matter and sediments traces terrigenous organic matter input. Geochimica et CosmochimicaActa, i-In press. Doi: 10.1016/j.gca.2015.11.008

Dittmers, K., Niessen, F., Stein, R., 2008. Late Weichselian fluvial evolution on the southern Kara Sea Shelf, North Siberia. Global and Planetary Change 60, 327–350.

van Dongen, B.E., Semiletov, I., Weijers, J.W.H., Gustafsson, Ö., 2008. Contrasting lipid biomarker composition of terrestrial organic matter exported from across the Eurasian Arctic by the five great Russian Arctic rivers. Global Biogeochemical Cycles 22, GB1011.

Fairbanks, R.G., 1989. A 17,000-year glacio-eustatic sea level record: influence of glacial melting rates on the Younger Dryas event and deep-ocean circulation. Nature 342, 637–642.

Fernandes, M.B., Sicre, M.-A., 2000. The importance of terrestrial organic carbon inputs on Kara Sea shelves as revealed by n-alkanes, OC and $\delta^{13}C$ values. Organic Geochemistry 31, 363–374.

Gardner, J.V., Dean, W.E., Klise, D.H., Baldauf, J.G., 1982. A climate-related oxidizing event in deep-sea sediment from the Bering Sea. Quaternary Research 18, 91–107.

Guo, L., Semiletov, I., Gustafsson, Ö., Ingri, J., Andersson, P., Dudarev, O., White, D., 2004. Characterization of Siberian Arctic coastal sediments: Implications for terrestrial organic carbon export. Global Biogeochemical Cycles 18, GB1036.

Gustafsson,Ö., van Dongen, B.E., Vonk, J. E., Dudarev, O.V.,Semiletov, I.P., 2011.Widespread release of old carbon across the Siberian Arctic echoed by its large rivers. Biogeosciences 8, 1737–1743.

Hald, M., Kolstad, V., Polyak, L., Forman, S.L., Herlihy, F.A., Ivanov, G., Nescheretov, A., 1999. Late-glacial and Holocene paleoceanography and sedimentary environments in the St. Anna Trough, Eurasian Arctic Ocean margin. Palaeogeography, Palaeoclimatology, Palaeoecology 146, 229–249.

Hanzlick, D., Aagaard, K., 1980. Freshwater and Atlantic water in the Kara Sea. Journal of Geophysical Research 85, 4937.

Huguet, C., de Lange, G.J., Gustafsson, O., Middelburg, J.J., Sinninghe Damsté, J.S., Schouten, S., 2008. Selective preservation of soil organic matter in oxidized marine sediments (Madeira Abyssal Plain). Geochimica et CosmochimicaActa 72, 6061–6068.

Hopmans, E.C., Weijers, J.W.H., Schefuß, E., Herfort, L., Sinninghe Damsté, J.S., Schouten, S., 2004. A novel proxy for terrestrial organic matter in sediments based on branched and isoprenoidtetraether lipids. Earth and Planetary Science Letters 224, 107–116.

Jakobsson, M., Mayer, L., Coakley, B., Dowdeswell, J.A., Forbes, S., Fridman, B., Hodnesdal, H., Noormets, R., Pedersen, R., Rebesco, M., Schenke, H.W., Zarayskaya, Y., Accettella, D., Armstrong, A., Anderson, R.M., Bienhoff, P., Camerlenghi, A., Church, I., Edwards, M., Gardner, J.V., Hall, J.K., Hell, B., Hestvik, O., Kristoffersen, Y., Marcussen, C., Mohammad, R., Mosher, D., Nghiem, S.V., Pedrosa, M.T., Travaglini, P.G., Weatherall, P., 2012. The International Bathymetric Chart of the Arctic Ocean (IBCAO) Version 3.0. Geophysical Research Letters 39, L12609.

Jakobsson, M., Andreassen, K., Bjarnadóttir, L.R., Dove, D., Dowdeswell, J.A., England, J.H., Funder, S., Hogan, K., Ingólfsson, Ó., Jennings, A., Krog Larsen, N., Kirchner, N., Landvik, J.Y., Mayer, L., Mikkelsen, N., Möller, P., Niessen, F., Nilsson, J., O'Regan, M., Polyak, L., Nørgaard-Pedersen, N., Stein, R., 2014. Arctic Ocean glacial history. Quaternary Science Reviews, APEX II: Arctic Palaeoclimate and its Extremes 92, 40–67.

Kim, J.-H., Schouten, S., Bonnin, J., Buscail, R., Ludwig, W., Sinninghe Damsté, J.S., Bourrin, F., 2006. Origin and distribution of terrestrial organic matter in the NW Mediterranean (Gulf of Lions): Exploring the newly developed BIT index. Geochemistry, Geophysics, Geosystems 7 11, Q11017.

Kim, J.-H., Zell, C., Moreira-Turcq, P., Perez, M.A.P., Abril, G., Mortillaro, J.-M., Weijers, J.W.H., Meziane, T., Sinninghe Damsté, J.S., 2012. Tracing soil organic carbon in the lower Amazon River and its tributaries using GDGT distributions and bulk organic matter properties. Geochimica et Cosmochimica Acta 90, 163–180.

Kleiber, H.P., Niessen, F., 2000. Variations of continental discharge pattern in space and time: implications from the Laptev Sea continental margin, Arctic Siberia. International Journal of Earth Sciences 89, 605–616.

Krishnamurthy, R.V., Machavaram, M., Baskaran, M., Brooks, J.M., Champ, M.A., 2001. Organic carbon flow in the Ob, Yenisey Rivers and Kara Sea of the Arctic Region. Marine Pollution Bulletin 42, 726–732.

Lein, A.Y., Kravchishina, M.D., Politova, N.V., Savvichev, A.S., Veslopolova, E.F., Mitskevich, I.N., Ul'yanova, N.V., Shevchenko, V.P., Ivanov, M.V., 2012. Transformation of particulate organic matter at the water-bottom boundary in the Russian Arctic seas: Evidence from isotope and radioisotope data. Lithology and Mineral Resources 47, 99–128.

Lengger, S.K., Kraaij, M., Tjallingii, R., Baas, M., Stuut, J.-B., Hopmans, E.C., Sinninghe Damsté, J.S., Schouten, S., 2013. Differential degradation of intact polar and core glycerol dialkyl glycerol tetraether lipids upon post-depositional oxidation. Organic Geochemistry 65, 83-93.

Mariotti, A., Lancelot, C., Billen, G., 1984. Natural isotopic composition of nitrogen as a tracer of origin for suspended organic matter in the Scheldt estuary. Geochimica et Cosmochimica Acta 48, 549–555.

Midttun, L., 1985. Formation of dense bottom water in the Barents Sea. Deep Sea Research Part A. Oceanographic Research Papers 32, 1233–1241.

Niemann, H., Stadnitskaia, A., Wirth, S.B., Gilli, A., Anselmetti, F.S., Sinninghe Damsté, J.S., Schouten, S., Hopmans, E.C., Lehmann, M.F., 2012. Bacterial GDGTs in Holocene sediments and catchment soils of a high Alpine lake: application of the MBT/CBT-paleothermometer. Climate of the Past 8, 889–906.

Peterse, F., Prins, M.A., Beets, C.J., Troelstra, S.R., Zheng, H., Gu, Z., Schouten, S., Sinninghe Damsté, J.S., 2011. Decoupled warming and monsoon precipitation in East Asia over the last deglaciation. Earth and Planetary Science Letters 301, 256–264.

Polukhin, A.A., Makkaveev, P., 2014. Long-term dynamics of pH and total alkalinity in the Kara Sea. In: Abstract Volume Arctic Ocean acidification, Bergen, Norway, 27.

Polyak, L., Forman, S.L., Herlihy, F.A., Ivanov, G., Krinitsky, P., 1997. Late Weichselian deglacial history of the Svyataya (Saint) Anna Trough, northern Kara Sea, Arctic Russia. Marine Geology 143, 169–188.

Polyak, L., Levitan, M., Gataullin, V., Khusid, T., Mikhailov, V., Mukhina, V., 2000. The impact of glaciation, river-discharge and sea-level change on Late Quaternary environments in the southwestern Kara Sea. International Journal of Earth Sciences 89, 550–562.

Prahl, F.G., Cowie, G.L., de Lange, G.J., Sparrow, M.A., 2003. Selective organic matter preservation in "burn-down" turbidites on the Madeira Abyssal Plain. Paleoceanography 18, 30-1.

Robinson, R.S., Kienast, M., Luiza Albuquerque, A., Altabet, M., Contreras, S., De Pol Holz, R., Dubois, N., Francois, R., Galbraith, E., Hsu, T.-C., Ivanochko, T., Jaccard, S., Kao, S.-J., Kiefer, T., Kienast, S., Lehmann, M., Martinez, P., McCarthy, M., Möbius, J., Pedersen, T., Quan, T.M., Ryabenko, E., Schmittner, A., Schneider, R., Schneider-Mor, A., Shigemitsu, M., Sinclair, D.,

Formatted: Highlight

Somes, C., Studer, A., Thunell, R., Yang, J.-Y., 2012. A review of nitrogen isotopic alteration in marine sediments. Paleoceanography 27, PA4203.

Schouten, S., Huguet, C., Hopmans, E.C., Kienhuis, M.V.M., Sinninghe Damsté, J.S., 2007. Analytical methodology for TEX_{86} paleothermometry by high performance liquid chromatography/atmospheric pressure chemical ionization-mass spectrometry. Analytical Chemistry 79, 2940–2944.

Schouten, S., Ossebaar, J., Brummer, G.J., Elderfield, H., Sinninghe Damsté, J.S., 2007. Transport of terrestrial organic matter to the deep North Atlantic Ocean by ice rafting. Organic Geochemistry 38, 1161–1168.

Shepard, F.P., 1954. Nomenclature based on sand-silt-clay ratios. Journal of Sedimentary Research 24, 151–158.

Sparkes, R.B., Doğrul Selver, A., Bischoff, J., Talbot, H. M., Gustafsson, Ö., Semiletov, I.P., Dudarev, O.V., van Dongen, B.E., 2015. GDGT distributions in the East Siberian Sea: implications for organic carbon export, burial and degradation. Biogeosciences 12, 637–674.

Sinninghe Damsté, J.S., Hopmans, E.C., Pancost, R.D., Schouten, S., Geenevasen, J.A.J., 2000. Newly discovered non-isoprenoid glycerol dialkyl glycerol tetraether lipids in sediments. Chemical Communications 1683–1684.

Stein, R., Dittmers, K., Fahl, K., Kraus, M., Matthiessen, J., Niessen, F., Pirrung, M., Polyakova, Y., Schoster, F., Steinke, T., Fütterer, D.K., 2004. Arctic (palaeo) river discharge and environmental change: evidence from the Holocene Kara Sea sedimentary record. Quaternary Science Reviews, 23, 1485–1511.

Tarasov, P.E., Peyron, O., Guiot, J., Brewer, S., Volkova, V.S., Bezusko, L.G., Dorofeyuk, N.I., Kvavadze, E.V., Osipova, I.M., Panova, N.K., 1999. Last Glacial Maximum climate of the former Soviet Union and Mongolia reconstructed from pollen and plant macrofossil data. Climate Dynamics 15, 227–240.

Tarasov, P.E., Bezrukova, E.V., Krivonogov, S.K., 2009. Late Glacial and Holocene changes in vegetation cover and climate in southern Siberia derived from a 15 kyr long pollen record from Lake Kotokel. Climate of the Past, 5, 285-295.

Thornton, S.F., McManus, J., 1994. Application of organic carbon and nitrogen stable isotope and C/N ratios as source indicators of organic matter provenance in estuarine systems: Evidence from the Tay Estuary, Scotland. Estuarine, Coastal and Shelf Science 38, 219–233.

Turner, R.R., Harriss, R.C., 1970. The distribution of non-detrital iron and manganese in two cores from the Kara Sea. Deep Sea Research and Oceanographic Abstracts 17, 3, 633–636.

Vetrov, A.A., Romankevich, E.A., 2011. Genesis of organic matter in the Kara Sea bottom sediments. Oceanology 51, 608–615.

Weijers, J.W.H., Schouten, S., Hopmans, E.C., Geenevasen, J.A.J., David, O.R.P., Coleman, J.M., Pancost, R.D., Sinninghe Damsté, J.S., 2006. Membrane lipids of mesophilic anaerobic bacteria thriving in peats have typical archaeal traits. Environmental Microbiology 8, 648–657.

Weijers, J.W.H., Schouten, S., van den Donker, J.C., Hopmans, E.C., Sinninghe Damsté, J.S., 2007a. Environmental controls on bacterial tetraether membrane lipid distribution in soils. Geochimica et CosmochimicaActa 71, 703–713.

Weijers, J.W.H., Schefuss, E., Schouten, S., Sinninghe Damsté, J.S., 2007b. Coupled thermal and hydrological evolution of tropical Africa over the last deglaciation. Science 315, 1701–1704.

Weijers, J.W.H., Schouten, S., Schefuß, E., Schneider, R.R., Sinninghe Damsté, J.S., 2009. Disentangling marine, soil and plant organic carbon contributions to continental margin sediments: A multi-proxy approach in a 20,000 year sediment record from the Congo deep-sea fan. Geochimica et Cosmochimica Acta 73, 119–132.

Formatted: Highlight

759 Weijers J.W.H., Schefuss E., Kim J.-H., Sinninghe Damsté, J.S., Schouten S., 2014. Constraints on the
760 sources of branched tetraether membrane lipids in distal marine sediments. Organic
761 Geochemistry, 72, 14-22.

762 Zech, R., Gao, L., Tarozo, R., Huang, Y., 2012. Branched glycerol dialkyl glycerol tetraethers in
763 Pleistocene loess-paleosol sequences: Three case studies. Organic Geochemistry 53, 38–44.

764 Zell, C., Kim, J.-H., Moreira-Turcq, P., Abril, G., Hopmans, E.C., Bonnet, M.-P., Sobrinho, R.L.,
765 Sinninghe Damsté, J.S., 2013. Disentangling the origins of branched tetraether lipids and
766 crenarchaeol in the lower Amazon river: Implications for GDGT-based proxies. Limnology and
767 Oceanography 58, 343–353.

768 Zell, C., Kim, J.-H., Balsinha, M., Dorhout, D., Fernandes, C., Baas, M., Sinninghe Damsté, J.S., 2014.
769 Transport of branched tetraether lipids from the Tagus River basin to the coastal ocean of the
770 Portuguese margin: Consequences for the interpretation of the MBT'/CBT paleothermometer.
771 Biogeosciences 11, 5637-5655.
772

Table 1

Fractional abundance~~s~~ and concentration of brGDGTs down-core in St. Anna Trough sediments and resulting proxy values~~.~~.

Unit	Depth (cm bsf)	Fractional abundance Ia	Ib	Ic	IIa	IIb	IIc	IIIa	IIIb	IIIc	IIa'	IIb'	IIc'	IIIa'	IIIb'	IIIc'	$PC1_{SAT}$[a]	$PC2_{SAT}$[a]	BrGDGTs (µg/g TOC)	Crenarchaeol (µg/g TOC)	BIT	IR	pH	MAT (°C)
1	1	23	5	2	10	3	1	11	1	0	7	11	4	15	4	2	-1.8	0.3	9	80	0.07	0.38	7.2	11
	10	24	5	2	10	1	1	13	1	0	7	12	4	16	2	1	-1.4	0.4	11	120	0.06	0.40	7.1	11
	18	16	37	2	7	1	1	8	1	0	5	9	3	9	1	1	-1.1	0.1	9	81	0.05	0.39	7.1	11
	40	18	24	3	8	1	1	9	1	0	6	12	4	12	2	1	-1.4	-0.1	15	140	0.05	0.36	7.2	11
	60	19	19	2	11	2	1	10	1	0	6	12	3	11	2	1	-1.3	-0.1	15	140	0.06	0.41	7.1	9
	80	20	9	3	13	2	1	13	1	0	7	14	3	9	2	2	-1.5	-0.3	12	100	0.07	0.45	7.1	8
	100	20	17	3	10	4	1	11	1	0	6	11	4	8	2	1	-1.4	-0.4	17	190	0.05	0.46	7.1	10
	120	21	22	2	12	3	1	9	1	0	8	9	3	7	2	1	-0.9	0.1	20	100	0.11	0.47	6.9	9
	125	24	17	2	15	2	0	10	1	0	10	7	3	8	1	1	-0.5	0.6	15	48	0.17	0.48	6.9	9
	130	25	12	1	16	4	0	11	1	0	13	4	2	9	1	0	-0.1	1	8	24	0.20	0.52	6.8	9
2a	137	28	11	1	18	2	0	12	0	0	14	3	1	9	1	0	0.4	1.2	7	6	0.45	0.55	6.7	8
2b	142	26	6	1	22	3	0	16	0	0	11	3	1	9	1	0	0.4	1.3	10	5	0.65	0.63	6.5	6
2c	146	30	5	1	23	3	0	15	0	0	10	3	1	7	1	0	0.4	0.8	26	9	0.71	0.65	6.4	7
2d	148	34	10	2	20	3	1	13	0	0	6	2	1	6	1	0	0.3	-0.3	13	9	0.53	0.70	6.2	9
	150	56	6	3	13	3	1	8	0	0	0	2	1	5	1	0	0.3	-2.6	12	12	0.44	0.76	5.8	16
	153	49	8	4	17	3	1	6	0	0	4	2	0	4	1	0	0.3	-2.1	8	7	0.47	0.72	6.0	13
2e	155	31	13	2	20	3	0	13	0	0	8	2	1	6	0	0	0.3	0.1	20	11	0.59	0.69	6.3	8
	160	35	3	2	26	3	0	13	0	0	9	2	0	6	0	0	0.7	0.3	28	4	0.87	0.71	6.2	8
	170	31	6	1	25	3	0	15	0	0	9	2	0	6	0	0	0.6	0.6	34	7	0.81	0.71	6.3	7
	180	30	5	1	25	3	0	16	0	0	9	2	0	6	0	0	0.6	0.7	44	9	0.81	0.71	6.3	7
	190	30	2	1	26	3	0	18	0	0	8	2	0	7	0	0	0.6	0.7	57	12	0.80	0.74	6.2	6
	200	29	2	1	26	3	0	19	0	0	8	2	0	7	0	0	0.6	0.9	20	5	0.79	0.73	6.2	6
3	210	31	5	1	26	3	0	15	0	0	9	2	0	6	0	0	0.7	0.6	26	5	0.81	0.71	6.2	7
	215	36	7	2	24	3	1	15	0	0	6	1	0	5	0	0	0.6	-0.4	7	3	0.71	0.76	6.1	8
	234	38	6	2	23	2	1	13	0	0	7	2	0	5	0	0	0.5	-0.4	15	3	0.79	0.74	6.1	9
	244	37	6	2	24	2	1	14	0	0	7	1	0	5	1	0	0.6	-0.4	15	4	0.76	0.74	6.1	9
	254	36	8	2	24	3	1	14	0	0	6	1	0	5	0	0	0.6	-0.5	28	9	0.73	0.76	6.1	8
	264	38	7	2	24	3	1	14	0	0	6	1	0	4	0	0	0.6	-0.7	12	5	0.68	0.77	6.0	9
	269	38	7	2	25	3	1	13	0	0	4	1	0	4	0	0	0.5	-0.9	16	6	0.70	0.81	5.9	8
	274	37	5	2	25	2	1	15	0	0	6	1	0	5	1	0	0.6	-0.3	10	3	0.73	0.76	6.0	8

284	36	6	2	24	2	0	14	0	0	7	2	0	5	1	0	0.6	-0.2	20	5	0.78	0.73	6.1	8
292	35	6	2	24	3	0	14	0	0	8	2	0	6	0	0	0.5	0	23	6	0.77	0.72	6.2	8

[a] Score on first 2 PCs of PCA_{SAT}.

EDITOR :THIS TABLE SHOULD BE THE ONE IN THE SUPPLEMENTARY MATERIAL

Supplementary Table 1

Bulk OM characteristics of samples.

Unit	Depth (cm, bsf)	TOC (%)	TN (%)	C/N	$\delta^{13}C_{org}$ (‰)	$\delta^{15}N$ (‰)
1	1	1.25	0.17	8	-22.8	5.1
	10	1.25	0.16	8	-23.1	5.2
	18	1.21	0.15	8	-23.4	5.3
	40	1.06	0.13	8	-23.4	5.3
	60	0.63	0.08	8	-24.2	4.7
	80	0.94	0.07	13	-24.5	3.3
	100	0.79	0.07	12	-25.7	3.4
	120	0.57	0.06	10	-24.6	2.4
	125	0.54	0.05	10	-25.0	3.0
	130	1.03	0.06	17	-24.6	3.3
2a	137	0.82	0.10	8	-24.1	5.2
2b	142	1.54	0.08	19	-24.7	3.8
2c	146	0.64	0.05	12	-25.9	4.1
2d	148	0.68	0.06	12	-25.9	4.0
	150	0.63	0.06	11	-25.2	3.4
	153	0.80	0.05	15	-24.8	3.7
2e	155	0.97	0.12	8	-23.9	5.4
	160	0.86	0.06	15	-24.8	3.7
	170	0.67	0.05	12	-25.0	3.7
	180	0.57	0.06	10	-25.0	3.5
	190	0.47	0.05	9	-25.2	3.4
	200	1.45	0.08	19	-24.5	3.6
3	210	0.84	0.06	14	-24.7	4.0
	215	1.28	0.16	8	-23.2	5.3
	234	1.09	0.12	9	-23.8	5.8
	244	0.69	0.09	8	-24.5	5.4
	254	0.31	0.04	7	-24.7	5.3
	264	0.44	0.05	10	-25.6	4.6
	269	0.52	0.05	10	-25.5	3.9
	274	0.70	0.06	12	-26.1	4.0
	284	0.72	0.06	12	-26.2	3.9
	292	0.68	0.06	12	-26.1	4.0

Formatted: Highlight

Figures

Fig. 1. Structures of brGDGTs (I-III) and crenarchaeol (IV). The structures of the hexa- and pentamethylated brGDGTs with cyclopentyl moiety(ies) IIb', IIc', IIIb' and IIIc' are tentatively assigned.

Fig. 2. (A) Bathymetric map of the Arctic Ocean, showing the location of the Kara Sea, modified after Jakobsson et al. (2012). (B) Map showing bathymetry of central part of the Kara Sea, with approximate boundaries of the St. Anna Trough indicated. The location of the core site is indicated by "N9". (C) Map showing current distribution of land masses (dark grea~~a~~y), with extent of the coastline during a sea level drop of 50 m, reflecting the conditions at 11 ka (Fairbanks, 1989; Bauch et al., 2001), indicated in light grea~~a~~y. The~~ei~~s map is simplified, as it is based on the current 50 m isobath, and assumes that isostatic rebound was negligible. The course of the palaeo Yenisei and Ob rivers is indicated with an arrow, after Stein et al. (2004).

Fig. 3. (A) Lithological description and sampled intervals. The sediments were sampled over an interval of 1 cm, and the top of each interval is indicated with a cross symbol. The arrows indicate characteristic horizons that allowed interpolation with dated horizons as reported by Polyak et al. (1997) or Hald et al. (1999) based on radiocarbon determinations reported in these studies. The colour and pattern per lithological unit, based on the Munsel colour scale and grain size classification, refers to the legend. Downcore distribution of (B) TOC content (%), (C) TN content (%)), (D) bulk C/N), (E) $\delta^{13}C_{org}$, (F) $\delta^{15}N$), (G) TOC-normalized concentration of summed brGDGTs (µg/g TOC), (H) TOC-normalized concentration of crenarchaeol (GDGT IV; µg/g TOC), (I) BIT index values (Eq. 1). The boundaries of the lithological units

and depths (cm below sea floor) are indicated on the scale on the left, yellow lines indicatinge the presence of oxidized lenses, based on lithological description.

Fig. 4. PCA based on standardized fractional abundances of the 15 brGDGTs in the St. Anna Trough core, plotting (A) the scores of the brGDGTs on the first two principal PCs. The scores of the downcore distributions are plotted vs. depth (cm bsf) in panel B and C. The IR values are plotted vs. depth in panel D. For B-D the depth (cm bsf) and boundaries of the lithological units are indicated on the scale on the left, and yellow lines indicate the presence of oxidized lenses, based on lithological description. Panels E-G show brGDGT distribution at three depths (1, 153 and 200 cm bsf) that are characteristic for the three end members of the brGDGT distributions in the core. The colour of the bars refers to the brGDGT structures, as reflected by the legend.

Fig. 5. PCA based on standardized fractional abundances of 15 brGDGTs in the trough core and the modern Yenisei and Kara Sea SPM, sediments, coastal cliff and soil samples, described by De Jonge et al. (2015a). Panel A shows the scores of the 15 brGDGTs on the first 2 PCs. Panel B shows the scores of the sites and depths. The downcore distributions are indicated with a number (1-3) that corresponds with the lithological unit, as defined in Fig. 3.

Fig. 6. (A) Downcore reconstructed soil pH (based on CBT', Eqs. 3 and 4) and (B) reconstructed MAT) (based on the MAT_{mrs}, Eq. 5]). Scale on the left indicates depth (cm bsf) and the lithological units as described in Fig. 3, and yellow lines indicate the presence of oxidized lenses, based on lithological description.

Figure 1

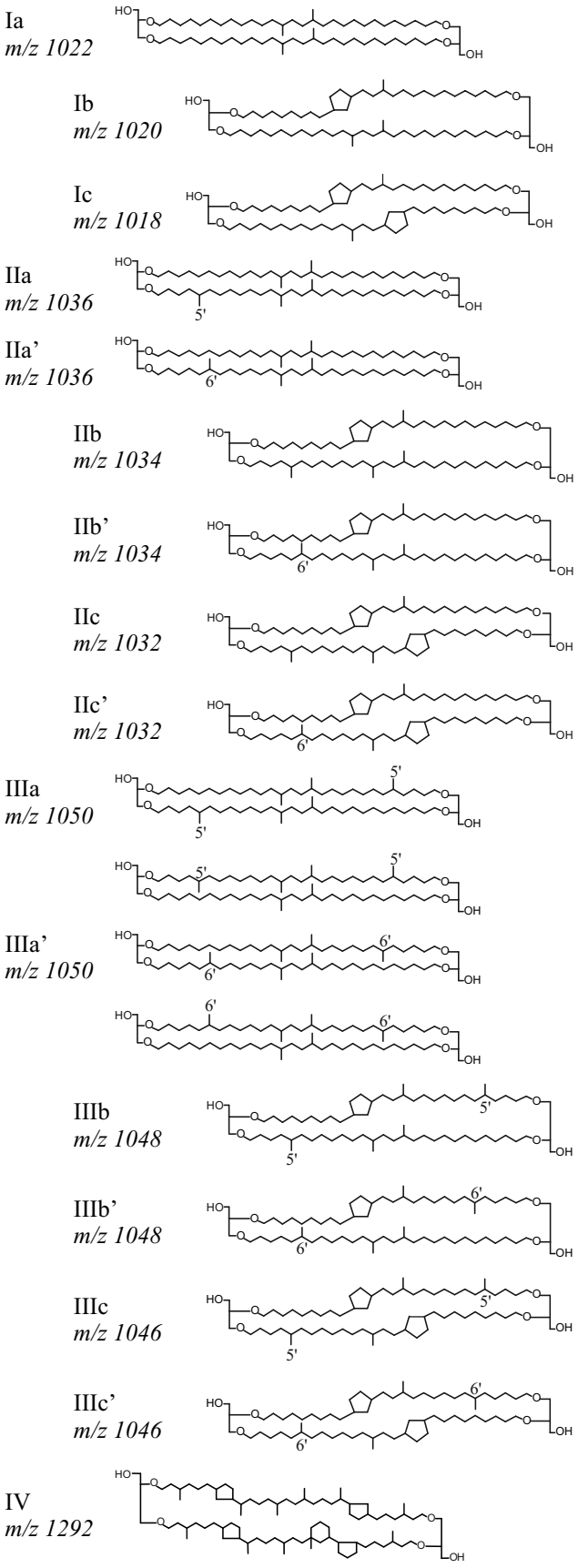
Ia
m/z 1022
Ib
m/z 1020
Ic
m/z 1018
IIa
m/z 1036
IIa'
m/z 1036
IIb
m/z 1034
IIb'
m/z 1034
IIc
m/z 1032
IIc'
m/z 1032
IIIa
m/z 1050
IIIa'
m/z 1050
IIIb
m/z 1048
IIIb'
m/z 1048
IIIc
m/z 1046
IIIc'
m/z 1046
IV
m/z 1292

Figure 2

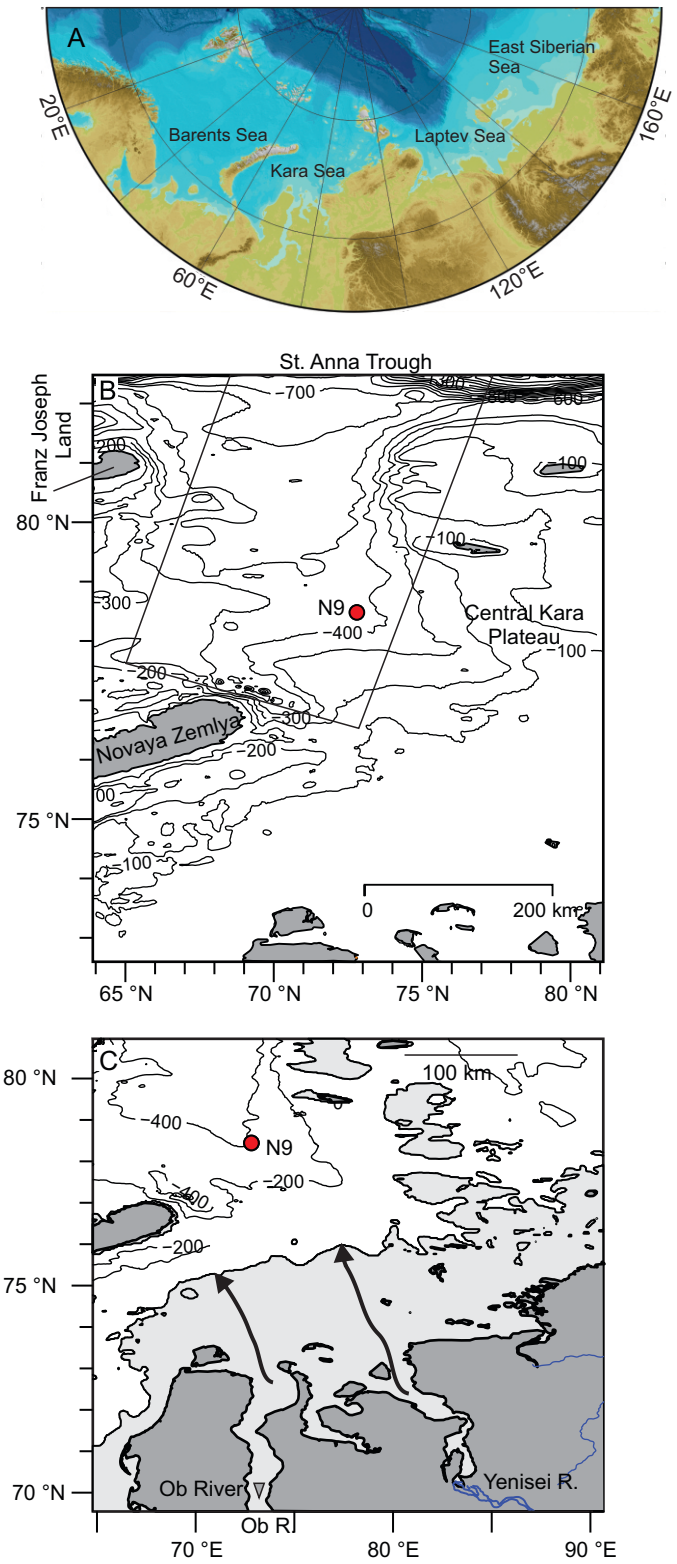
A
East Siberian Sea
Barents Sea
Laptev Sea
Kara Sea
20°E
160°E
60°E
120°E
St. Anna Trough
B
Franz Joseph Land
80 °N
75 °N
N9
Central Kara Plateau
Novaya Zemlya
0
200 km
65 °N
70 °N
75 °N
80 °N
C
100 km
N9
80 °N
75 °N
70 °N
Ob River
Yenisei R.
Ob R
70 °E
80 °E
90 °E

Figure 3

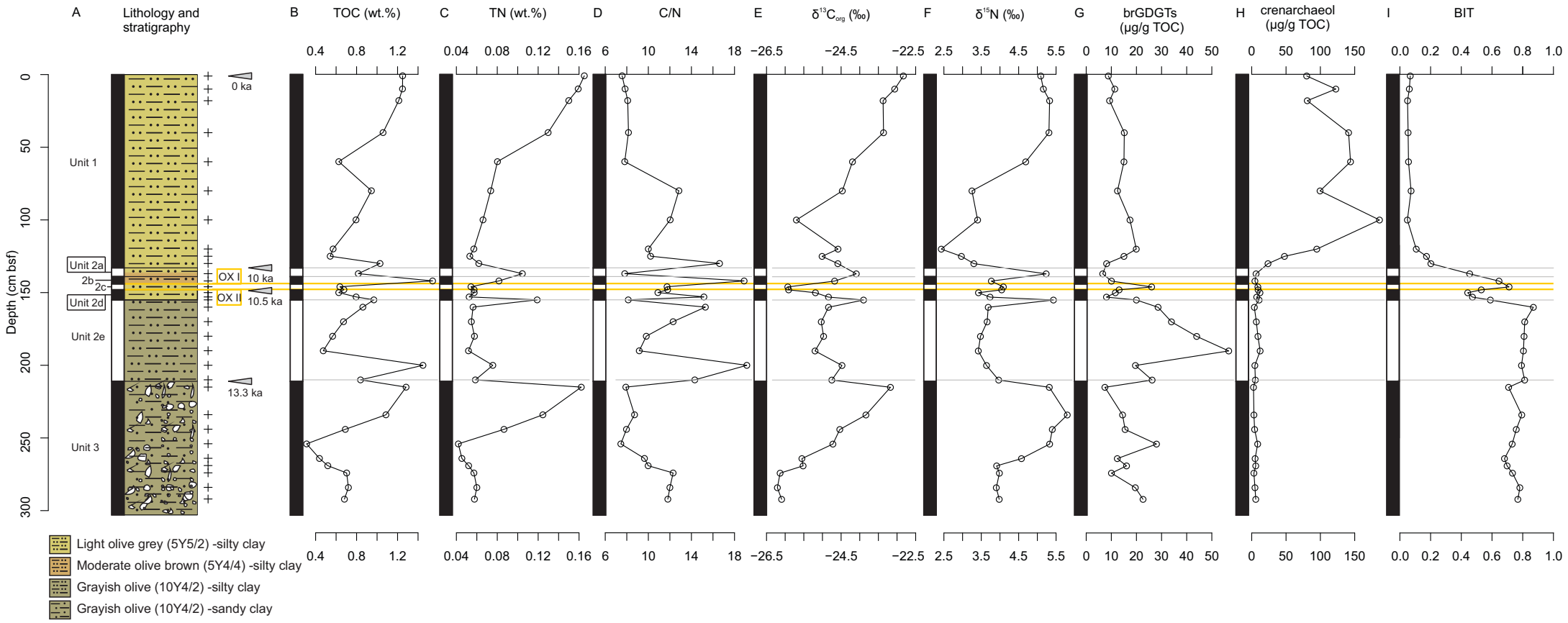
A
Lithology and stratigraphy
B
TOC (wt.%)
C
TN (wt.%)
D
C/N
E
δ13Corg (‰)
F
δ15N (‰)
G
brGDGTs (µg/g TOC)
H
crenarchaeol (µg/g TOC)
I
BIT
Depth (cm bsf)
0 ka
Unit 1
Unit 2a
2b
2c
Unit 2d
OX I
10 ka
OX II
10.5 ka
Unit 2e
13.3 ka
Unit 3
Light olive grey (5Y5/2) -silty clay
Moderate olive brown (5Y4/4) -silty clay
Grayish olive (10Y4/2) -silty clay
Grayish olive (10Y4/2) -sandy clay

Figure 4

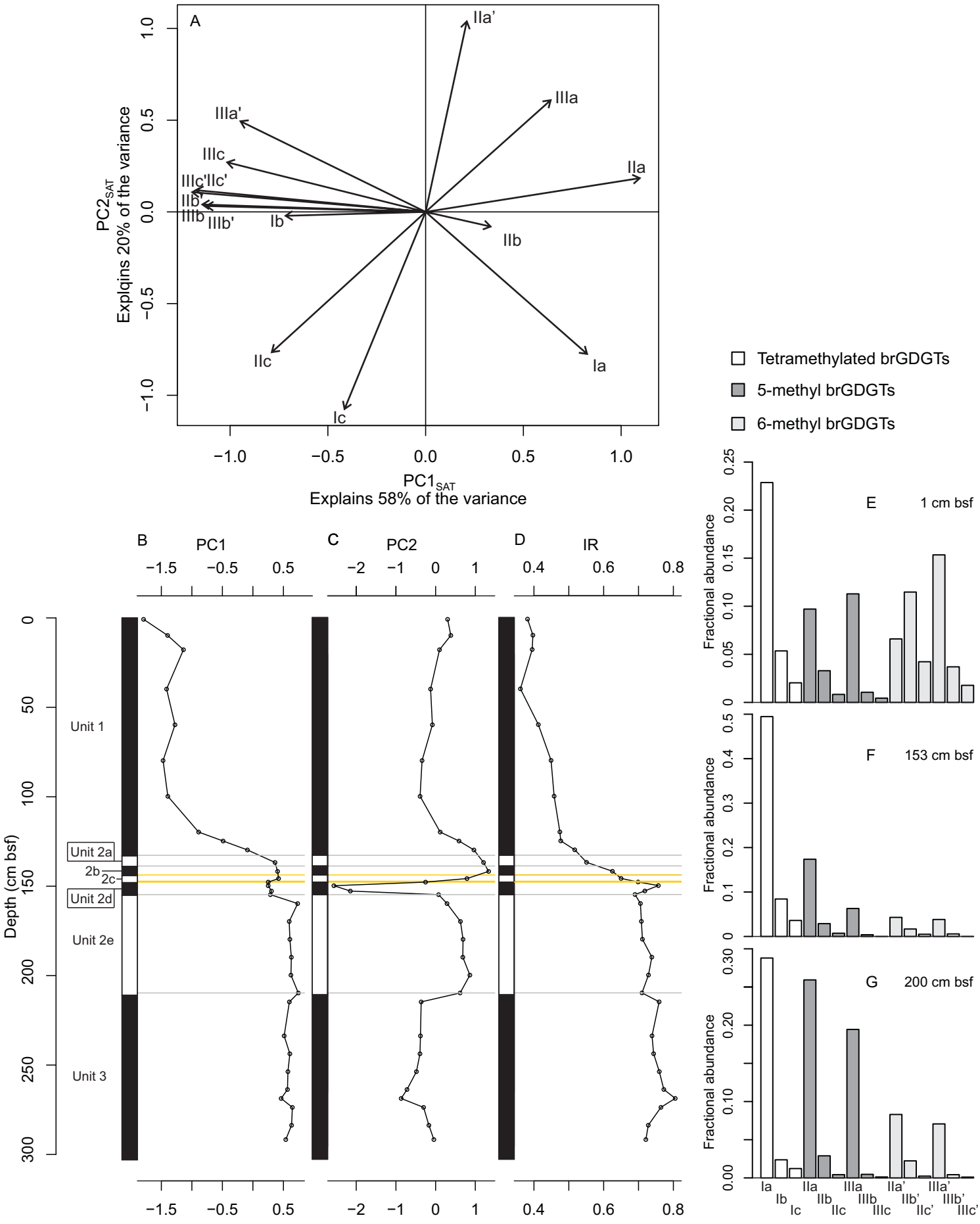
A
IIa'
IIIa
IIIa'
IIIc
IIa
IIIc'IIc'
IIb'
IIIb
IIIb'
Ib
IIb
IIc
Ia
Ic
PC2SAT
Explqins 20% of the variance
PC1SAT
Explains 58% of the variance
Tetramethylated brGDGTs
5-methyl brGDGTs
6-methyl brGDGTs
B
PC1
C
PC2
D
IR
Depth (cm bsf)
Unit 1
Unit 2a
2b
2c
Unit 2d
Unit 2e
Unit 3
E
1 cm bsf
F
153 cm bsf
G
200 cm bsf
Fractional abundance
Ia
Ib
Ic
IIa
IIb
IIc
IIIa
IIIb
IIIc
IIa'
IIb'
IIc'
IIIa'
IIIb'
IIIc'

Figure 5

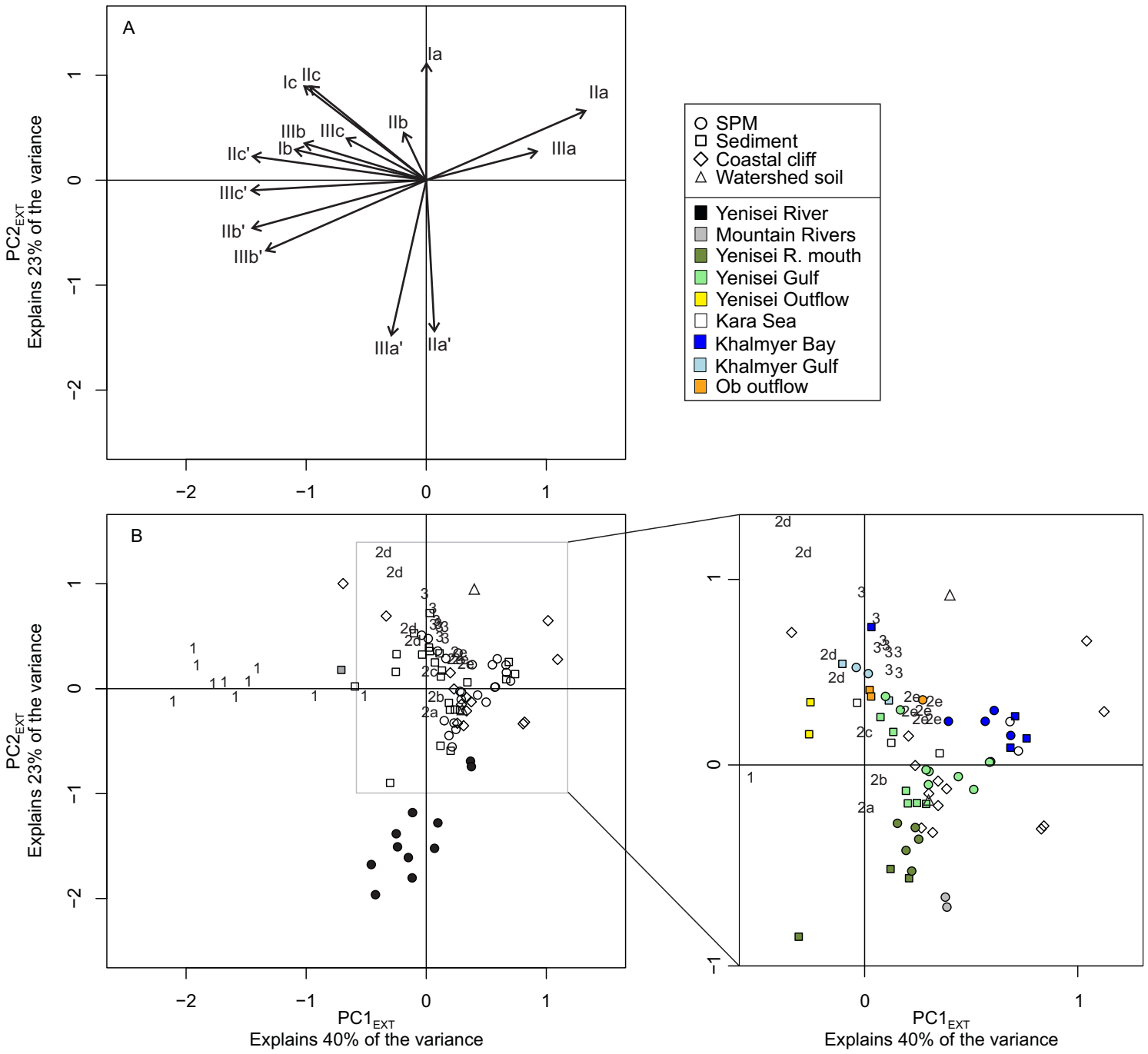
A
Ia
Ic
IIc
IIa
IIIb
IIIc
IIb
IIIa
IIc'
Ib
IIIc'
IIb'
IIIb'
IIIa'
IIa'
SPM
Sediment
Coastal cliff
Watershed soil
Yenisei River
Mountain Rivers
Yenisei R. mouth
Yenisei Gulf
Yenisei Outflow
Kara Sea
Khalmyer Bay
Khalmyer Gulf
Ob outflow
B
PC2EXT
Explains 23% of the variance
PC1EXT
Explains 40% of the variance

Figure 6

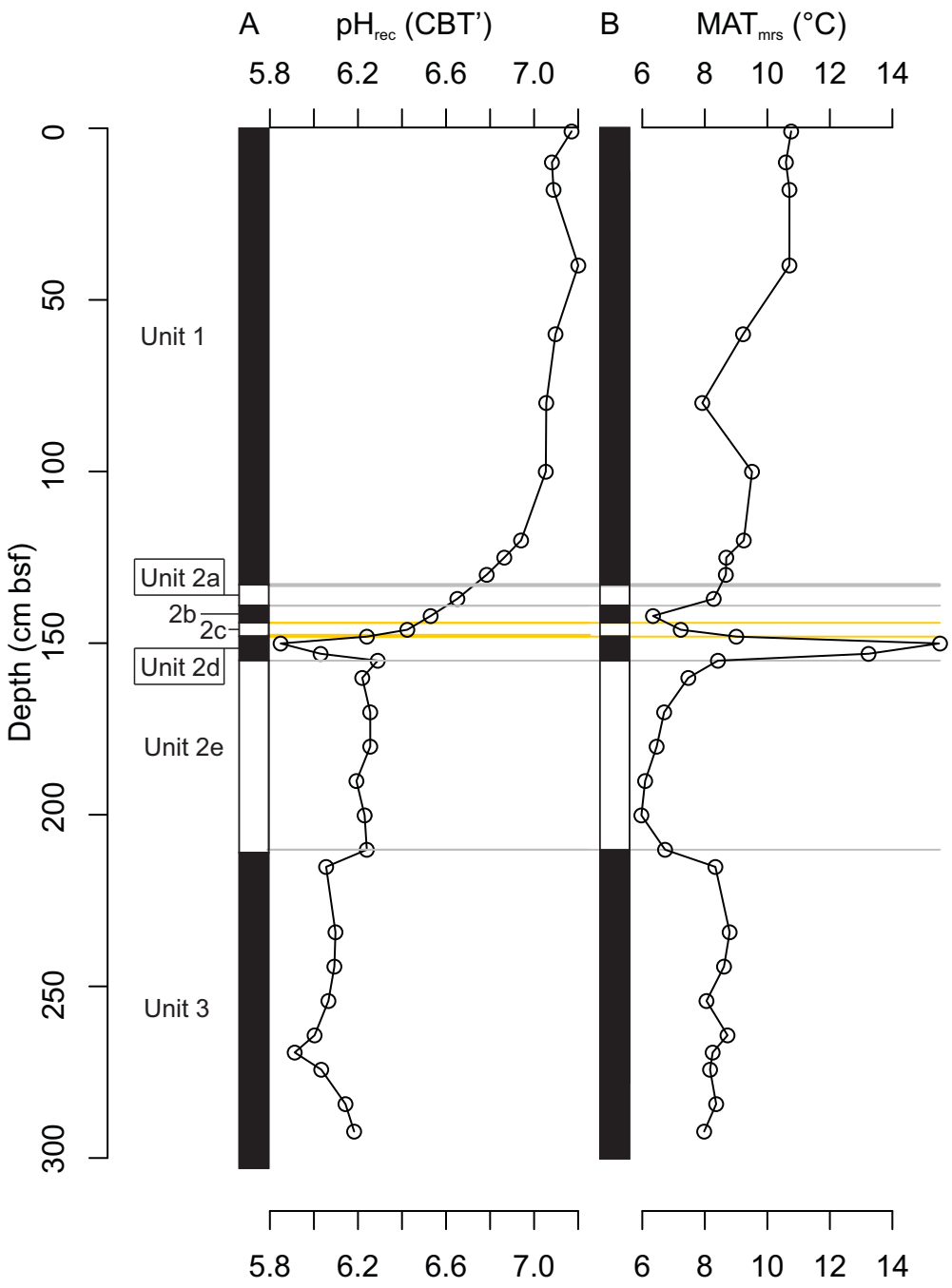
A
pH$_{rec}$ (CBT')
B
MAT$_{mrs}$ (°C)
5.8
6.2
6.6
7.0
6
8
10
12
14
Depth (cm bsf)
0
50
100
150
200
250
300
Unit 1
Unit 2a
2b
2c
Unit 2d
Unit 2e
Unit 3